CANCER

The tyrosine phosphatase PTPN14 (Pez) inhibits metastasis by altering protein trafficking

Leila Belle,[1,2]* Naveid Ali,[3]* Ana Lonic,[1,4]* Xiaochun Li,[1] James L. Paltridge,[1,2] Suraya Roslan,[1] David Herrmann,[5] James R. W. Conway,[5] Freya K. Gehling,[1] Andrew G. Bert,[1] Lesley A. Crocker,[1] Anna Tsykin,[1] Gelareh Farshid,[6] Gregory J. Goodall,[1,4,7] Paul Timpson,[5] Roger J. Daly,[3,8] Yeesim Khew-Goodall[1,2,4]†

Factors secreted by tumor cells shape the local microenvironment to promote invasion and metastasis, as well as condition the premetastatic niche to enable secondary-site colonization and growth. In addition to this secretome, tumor cells have increased abundance of growth-promoting receptors at the cell surface. We found that the tyrosine phosphatase PTPN14 (also called Pez, which is mutated in various cancers) suppressed metastasis by reducing intracellular protein trafficking through the secretory pathway. Knocking down PTPN14 in tumor cells or injecting the peritoneum of mice with conditioned medium from PTPN14-deficient cell cultures promoted the growth and metastasis of breast cancer xenografts. Loss of catalytically functional PTPN14 increased the secretion of growth factors and cytokines, such as IL-8 (interleukin-8), and increased the abundance of EGFR (epidermal growth factor receptor) at the cell surface of breast cancer cells and of FLT4 (vascular endothelial growth factor receptor 3) at the cell surface of primary lymphatic endothelial cells. We identified RIN1 (Ras and Rab interactor 1) and PRKCD (protein kinase C-δ) as binding partners and substrates of PTPN14. Similar to cells overexpressing PTPN14, receptor trafficking to the cell surface was inhibited in cells that lacked PRKCD or RIN1 or expressed a nonphosphorylatable RIN1 mutant, and cytokine secretion was decreased in cells treated with PRKCD inhibitors. Invasive breast cancer tissue had decreased expression of *PTPN14*, and patient survival was worse when tumors had increased expression of the genes encoding RIN1 or PRKCD. Thus, PTPN14 prevents metastasis by restricting the trafficking of both soluble and membrane-bound proteins.

INTRODUCTION

Metastasis, a multistep process in which cancer cells acquire invasive, migratory characteristics that enable them to escape the primary site and colonize secondary organs, is the main cause of death in breast cancer patients. Several studies have brought to light the enormous impact that the factors secreted by cancer cells—the secretome—has on both the local environment and distant sites to promote metastasis (*1*–*4*). Compared with their normal counterparts, cancer cells have a vastly different secretome (*5*, *6*) that can act in both an autocrine and paracrine manner to bring about a favorable outcome for the cancer cell. Tumor cells can secrete proangiogenic factors that promote the formation of new blood vessels, factors that recruit bone marrow–derived cells, which also contribute to promoting angiogenesis, and factors that promote extracellular matrix (ECM) remodeling through the activation of fibroblasts (*7*). It is also becoming clear that the cancer cell secretome can act distally to precondition secondary sites for colonization long before the cancer cells arrive (*3*, *4*). Furthermore, there is also evidence to support a role for the cancer cell secretome in influencing secondary-site tropism (*3*). Although the aberrant expression of genes encoding specific transcription factors (*8*, *9*) or microRNAs (*10*, *11*) has been considered as a contributing factor, the mechanisms regulating the cancer cell secretome are currently poorly characterized. A deeper understanding of the mechanisms used by tumor cells to convert their secretome profile from that of a nonmalignant cell to one that favors tumor progression and metastasis is therefore likely to be critical in combating metastatic disease.

PTPN14 (also known as Pez, PTPD2, PTP36) is a developmentally regulated nonreceptor protein tyrosine phosphatase (PTP) (*12*). Deficiency or loss of PTPN14 gives rise to developmental defects in zebrafish (*13*) and *Drosophila* (*14*) and to lymphedema in mice and humans (*15*). In addition, mutations in *PTPN14* are found in colorectal, breast, and liver cancers (*16*–*18*). However, the biological functions of PTPN14 and especially its substrates remain poorly characterized. To date, three PTPN14 substrates have been identified: β-catenin (*19*), YAP (Yes-associated protein) (*20*), and the docking protein p130Cas (*21*). We previously showed that PTPN14 localizes to either the nucleus or the cytoplasm in a cell density–dependent manner; in confluent endothelial cells, where it localizes to the adherens junctions, it regulates the Tyr phosphorylation status of these junctions, at least in part through its substrate β-catenin (*19*). When overexpressed in polarized MDCK (Madin-Darby canine kidney) epithelial cells, PTPN14 enhances transforming growth factor–β (TGFβ) secretion and, through the autocrine action of TGFβ, promotes an epithelial-to-mesenchymal transition (EMT) (*13*). In HeLa cells, overexpression of the mouse ortholog of PTPN14 altered cell morphology and the actin cytoskeleton and reduced cell-matrix adhesion (*22*). *Drosophila* Pez has been found to interact with KIBRA (kidney and brain expressed protein) as a component of the Hippo signaling pathway, restricting intestinal stem cell (ISC) proliferation (*14*),

[1]Centre for Cancer Biology, an Alliance between SA Pathology and University of South Australia, Adelaide, South Australia 5000, Australia. [2]Discipline of Biochemistry, School of Molecular and Biomedical Science, The University of Adelaide, Adelaide, South Australia 5005, Australia. [3]Cancer Research Program, Garvan Institute of Medical Research, Darlinghurst, New South Wales 2010, Australia. [4]Department of Medicine, The University of Adelaide, Adelaide, South Australia 5005, Australia. [5]Cancer Research Program, The Kinghorn Cancer Centre, Garvan Institute of Medical Research, Darlinghurst, New South Wales 2010, Australia. [6]Division of Tissue Pathology, SA Pathology, Adelaide, South Australia 5000, Australia. [7]School and Molecular and Biomedical Science, The University of Adelaide, Adelaide, South Australia 5005, Australia. [8]Department of Biochemistry and Molecular Biology, Monash University, Clayton, Victoria 3800, Australia.
*These authors contributed equally to this work.
†Corresponding author. E-mail: yeesim.khew-goodall@health.sa.gov.au

and human PTPN14 inhibits the oncogenic function of YAP (*20*, *23*–*25*), another member of the Hippo signaling pathway. Although some of the known functions of PTPN14 such as regulating the phosphorylation status of endothelial adherens junctions (*19*) are dependent on its phosphatase activity, others such as its role in restricting ISC proliferation are not (*14*). Here, we investigated the role of PTPN14 in breast cancer and used an unbiased approach to identify PTPN14 substrates.

RESULTS

PTPN14 suppresses the invasion and metastasis of triple-negative breast cancer cells in a xenograft breast cancer model

Mutations in *PTPN14* have been found in multiple cancers (*16*–*18*), although a direct role for Pez in cancer has yet to be shown. Because *PTPN14*-null humans, albeit a small cohort, do not appear to have a higher incidence of cancer (*15*), we reasoned that should PTPN14 play a role in breast cancer, it would most likely be in its progression rather than in tumor initiation. We investigated the possibility of a link between *PTPN14* expression and the progression from noninvasive to invasive tumors by comparing *PTPN14* mRNA abundance between ductal carcinomas in situ (DCIS) and invasive ductal carcinomas (IDC). We carefully macrodissected (*26*) the epithelial cells from both DCIS and IDC samples to minimize contamination with stromal cells lacking *PTPN14* expression. Although there was a 40-fold spread in *PTPN14* expression within the IDC cohort, the median *PTPN14* expression was significantly lower (3-fold) in IDC compared to DCIS (Fig. 1A), suggesting a loss of *PTPN14* expression as the cancer becomes invasive. This was somewhat surprising in light of our earlier finding that PTPN14 overexpression in epithelial cells induced an EMT (*13*) that would make the cells more invasive. Noting, however, the large range of *PTPN14* expression in IDC and that the signals for inducing EMT are non–cell-autonomous in many cancers, we asked whether reducing the amount of PTPN14 would have an effect on the invasiveness of cells that were already "mesenchymal" but had high PTPN14 abundance. The MDA-MB-231 breast cancer cell line exhibits a mesenchymal phenotype and a basal B gene expression signature (*27*) and has a basal abundance of PTPN14 (Fig. 1B). For ease of translation into a mouse cancer model, we used the LM2 derivative of this line (which is more metastatic and also expresses a luciferase reporter) (*28*). We introduced a short hairpin RNA (shRNA) that targets *PTPN14* mRNA (sh*PTPN14*) or control shRNA (shCon) into the LM2 cells and generated stable pools of LM2-sh*PTPN14* or LM2-shCon cell lines (Fig. 1B). The effect of PTPN14 knockdown on the invasiveness of LM2 cells was evaluated using an in vitro three-dimensional (3D) organotypic invasion assay (*29*), in which LM2-sh*PTPN14* or LM2-shCon cells were layered over a contracted collagen gel that was embedded with human mammary fibroblasts. Invasion into the collagen mimics the invasion of breast cancer cells through the mammary stroma in the early stages of cancer progression. PTPN14 knockdown significantly increased the number of cells that invaded into the matrix (Fig. 1, C and D). PTPN14 knockdown caused a small increase in the proliferation of cells sitting on top of the matrix but had no effect on cells that had invaded into the matrix (Fig. 1, E and F). A similar outcome was also obtained in MDA-MB-231 cells expressing sh*PTPN14* or shCon (fig. S1). Together with our finding that *PTPN14* expression is lower in invasive than in noninvasive breast cancer, these data suggest that loss of PTPN14 drives invasive breast cancer.

In breast cancer, the acquisition of invasive properties is a precursor to metastasis. We therefore investigated whether the abundance of PTPN14 affected metastasis in an orthotopic xenograft model of breast cancer using nonobese diabetic/severe combined immunodeficient (NOD/SCID) mice.

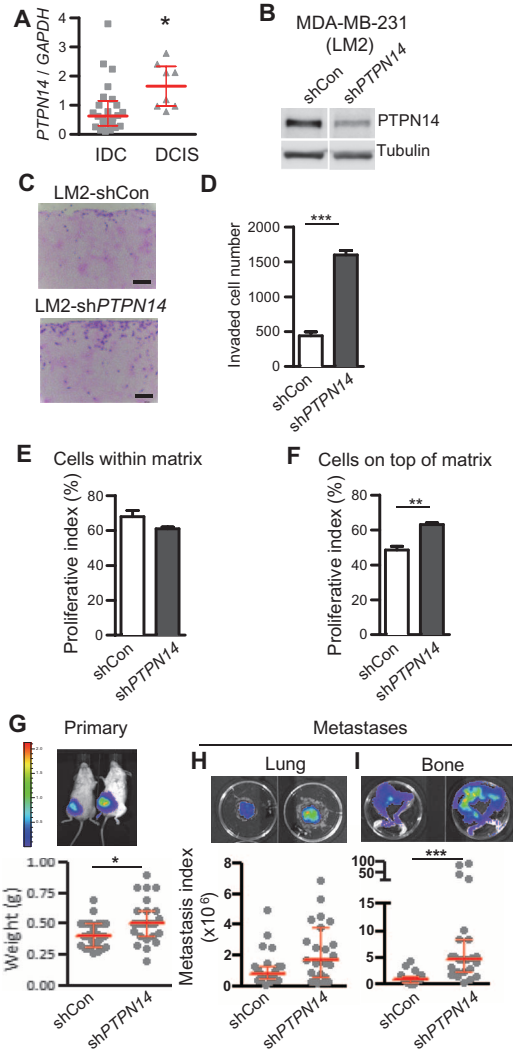

Fig. 1. Reducing the abundance of PTPN14 promotes invasiveness and metastasis in breast cancer. (**A**) Quantitative RT-PCR of *PTPN14* relative to glyceraldehyde-3-phosphate dehydrogenase (GAPDH) mRNA in tissue macrodissected from IDC and DCIS of the breast. $n = 24$ (IDC) or $n = 8$ (DCIS) patients. $^{*}P < 0.05$, Mann-Whitney *U* test. Red lines, median with interquartile range. (**B**) Western blotting for PTPN14 in whole-cell lysates from MDA-MB-231 (LM2) cells stably expressing a control vector (shCon) or shRNA to *PTPN14* (sh*PTPN14*). (**C** to **F**) Invasive capacity of control LM2 cells (LM2-shCon) and PTPN14-knockdown LM2 cells (LM2-sh*PTPN14*) assessed by 3D organotypic collagen I invasion assays. (C) Hematoxylin and eosin (H&E) staining of invasion assays at day 10. Scale bars, 100 μm. Images are representative of three experiments. (D to F) Quantification of invasion (D) and proliferation (E and F) as measured by Ki67 staining of cells within or on top of the matrix. Data are means ± SEM from three independent experiments. $^{***}P < 0.001$, $^{**}P < 0.01$, Student's *t* test. (**G** to **I**) Analysis of primary tumors (G) and lung or bone metastases (H and I) formed from LM2-shCon or LM2-sh*PTPN14* xenografts 4 to 5 weeks after orthotopic injection into the mammary fat pads of NOD/SCID mice. Top panels show representative bioluminescence images. Bottom panels show mass of primary tumors and quantitation of metastases as ex vivo bioluminescence normalized to primary tumor mass. Data are from ≥20 mice each. $^{**}P < 0.05$, $^{***}P < 0.001$, Mann-Whitney *U* test. Red lines, median with interquartile range.

Four to five weeks after injection of LM2-sh*PTPN14* or LM2-shCon cells into the mammary fat pad, the sizes of primary tumors were assessed by weight, and the presence of metastases in the lungs and long bones was analyzed by ex vivo bioluminescence imaging. There was a small but significant increase in the mass of the primary tumors arising from LM2-sh*PTPN14* cells compared with those arising from control cells (Fig. 1G), consistent with an increase in the proliferative capacity of PTPN14-deficient cells (Fig. 1F). The influence of primary tumor growth on metastasis was accounted for by quantifying the metastasis index (ratio of bioluminescence in secondary tumors to primary tumor mass) for each mouse. A modest but statistically insignificant increase in the median metastasis index was observed in lung metastasis (Fig. 1H), but a highly significant increase in bone metastasis was observed when PTPN14 was reduced (Fig. 1I). These data suggest that PTPN14 acts as a suppressor of metastasis, particularly to the metastatic niche in the bone.

PTPN14 modulates the secretome of breast cancer cells

Crosstalk between solid cancers and the surrounding tumor microenvironment through the production of growth factors, ECM proteins, proteases, and proangiogenic factors can have a profound influence on tumor growth and metastatic spread [reviewed in (*30*)]. Our previous findings that overexpression of PTPN14 increased the secretion of TGFβ from MDCK epithelial cells (*13*), which was recapitulated in breast cancer cell lines in this study (fig. S2), prompted us to investigate whether PTPN14 had a broader role in regulating protein trafficking and the secretion of soluble proteins other than TGFβ. To assess this, we overexpressed PTPN14 in MDA-MB-468 cells and knocked down PTPN14 in MDA-MB-231 cells (Fig. 2A). The relationship between PTPN14 abundance and protein secretion was determined in conditioned media from MDA-MB-468 cells expressing an empty vector (EV) or PTPN14 (468-EV and 468-PTPN14, respectively) or MDA-MB-231 cells expressing a control shRNA or *PTPN14* shRNA (231-shCon and 231-sh*PTPN14*, respectively) for 19 cytokines and growth factors that were arbitrarily selected using an antibody-based cytokine array (fig. S3). Eleven cytokines displayed reciprocal changes of greater than 20% from the respective controls both upon PTPN14 overexpression and upon PTPN14 knockdown, whereas the remaining eight cytokines either were unaltered or did not exhibit reciprocal changes upon manipulation of PTPN14 abundance (Fig. 2B). Confirmatory quantification of three arbitrarily selected cytokines [interleukin-6 (IL-6), IL-8, and vascular endothelial growth factor (VEGF)] with the Bio-Plex multiplex assay (Fig. 2C) showed good concordance with data obtained using the cytokine antibody array (Fig. 2B), and with the exception of VEGF in MDA-MB-468 cells, manipulating PTPN14 abundance resulted in about twofold changes in secreted protein for these cytokines. Quantitative reverse transcription polymerase chain reaction (RT-PCR) analysis showed no significant changes in the transcript abundance of the cytokines examined except MCP-1, IL-6, and angiogenin, whose mRNA abundance mirrored the changes in protein detected in the conditioned medium upon manipulation of PTPN14 (fig. S4). This indicated that, in general, PTPN14 did not regulate de novo synthesis of the cytokines examined; therefore, the changes in extracellular amounts of cytokines brought about by altering PTPN14 are most consistent with increased or decreased secretion of preexisting protein. For most of the cytokines that were affected by manipulating PTPN14 abundance, their secretion appeared to be suppressed by PTPN14.

PTPN14 suppresses the secretion of prometastatic factors

Secreted factors produced by cancer cells can modify the local microenvironment to facilitate invasion or they can modify distant naïve sites to favor colonization by cancer cells (*3*, *28*, *31*), both of which promote metastasis. This led us to examine whether the secretome of LM2-sh*PTPN14* cells can influence metastasis to secondary sites. Mice were given daily intraperitoneal injections of cell-free conditioned medium from either LM2-sh*PTPN14* or LM2-shCon cultures daily starting 3 days before injection of LM2-shCon cells until termination of the experiment (fig. S5). At 4 to 5 weeks after injection, no significant difference in the average

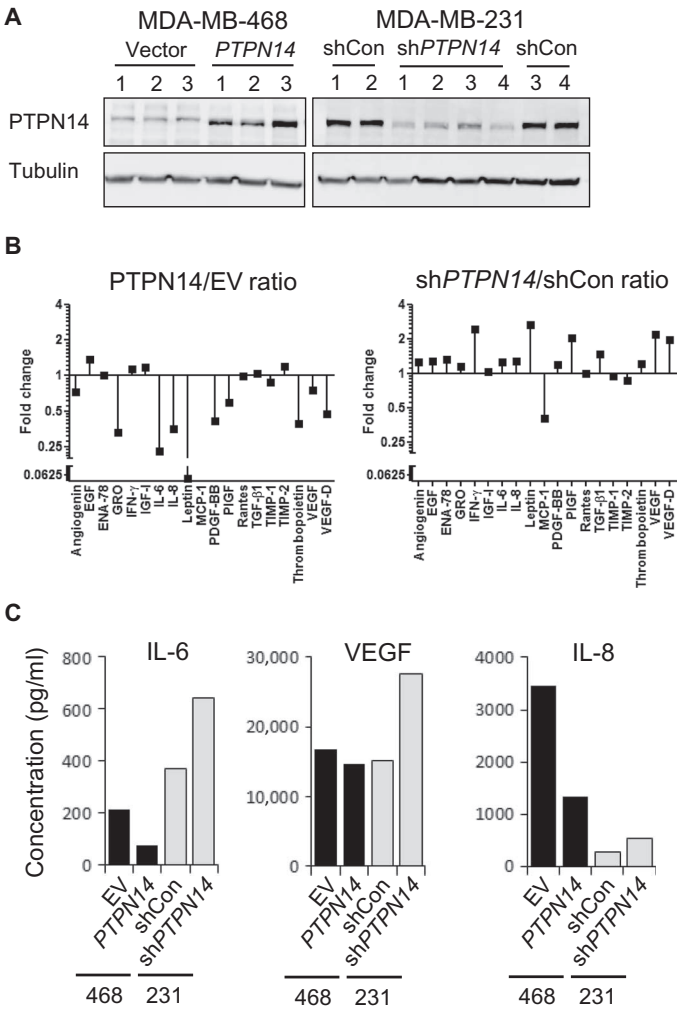

Fig. 2. Changes in PTPN14 abundance influence secretome composition. (**A**) Western blotting for PTPN14 in lysates from MDA-MB-468 and MDA-MB-231 clones. Blots are representative of at least three experiments. (**B**) Abundance of cytokines in pooled conditioned media (CM) from 468-EV relative to 468-PTPN14 (three independent clones each) and 231-shCon relative to 231-sh*PTPN14* clones (four independent clones each), determined by a cytokine antibody array. Fold change for MCP-1 could not be calculated; the amount of MCP-1 in 468-EV cells was below detection (raw data in fig. S3). $P = 0.002$, comparing ratios in the left panel with ratios in the right panel for 18 cytokines, by Wilcoxon matched pair analysis. (**C**) Abundance of IL-6, VEGF, and IL-8 in pooled CM from 468-EV, 468-PTPN14, 231-shCon, or 231-sh*PTPN14* clones, quantified using a multiplexed cytokine bead enzyme-linked immunosorbent assay (ELISA). Data show the mean from two independent clones from each cell line.

mass of primary LM2-shCon tumors was observed between mice injected with conditioned medium from PTPN14-deficient cells or control cells, but there was an increase in lung metastases and a significant increase in bone metastases of LM2-shCon cells when the mice were treated with LM2-sh*PTPN14*–conditioned medium compared with that from LM2-shCon cells (Fig. 3, A to C). This suggests that the conditioned medium from PTPN14-deficient cells injected into the peritoneum enhanced the metastasis of the control LM2 cells, which express endogenous amounts of PTPN14. Together, our data are consistent with the notion that the altered secretome of PTPN14-deficient cells drives their enhanced metastatic potential.

Quantitative phosphoproteomics identifies candidate PTPN14 substrates

The functional diversity of the three PTPN14 substrates identified to date [β-catenin (*19*), YAP (*20*), and p130Cas (*21*)] indicates that there may be more unidentified substrates. On the basis of the rationale that the inhibition of phosphatases causes increased phosphorylation of their substrates, we identified additional PTPN14 substrates using an unbiased approach [differential SILAC (stable isotope labeling with amino acids in cell culture) followed by nano-LC–MS/MS (nano-liquid chromatography–tandem mass spectrometry)] in which we isolated proteins that were differentially Tyr-phosphorylated in cells with low abundance of PTPN14 (231-sh*PTPN14*) compared with controls (231-shCon) (fig. S6, A and B). We identified 15 proteins (17 phosphosites) that had increased Tyr phosphorylation when PTPN14 was reduced (table S1), implicating them as candidate PTPN14 substrates. Another essential feature of a PTP substrate is its ability to interact, and thus coimmunoprecipitate, with the phosphatase; however, substrates that bind solely to the catalytic site of the phosphatase through their target phospho-Tyr residues are less readily isolated by coimmunoprecipitation because the substrate is released after catalysis. To overcome this, we used a substrate-trapping PTPN14 mutant [reviewed in (*32*)], in which the proton donor Asp and the nucleophile Cys are mutated to Ala and Ser, respectively, to generate a catalytically inactive mutant (D1079A/C1121S) that retains the ability to bind the substrate. We performed immunoprecipitations in human embryonic kidney (HEK) 293T cells coexpressing a selection of candidate substrates identified by our SILAC screen with Flag-tagged D1079A/C1121S-PTPN14 (ST-PTPN14, for substrate-trapping PTPN14) or an EV. Western blot analysis of the immunoprecipitates revealed that each of the candidate substrates tested [INPPL1 (SH2-containing inositol 5-phosphatase 2), RIN1 (Ras and Rab interactor 1), IRS1 (insulin receptor substrate 1), eEF1A1 (elongation factor 1 α1), TYK2 (tyrosine kinase 2), and PRKCD (protein kinase C-δ)] coimmunoprecipitated differentially with ST-PTPN14 (Fig. 4A). Western blot analysis of lysates from 231-shCon and 231-sh*PTPN14* cells indicated that, for these candidate substrates, there was no overt increase in protein abundance in PTPN14-deficient cells (fig. S7), indicating that the increase in amount of phosphopeptides detected by MS was due to an increase in degree of Tyr phosphorylation. Increased Tyr phosphorylation of specific residues within these proteins in cells that are hypomorphic for PTPN14, together with their ability to interact with PTPN14, suggests that INPPL1, RIN1, IRS1, eEF1A1, TYK2, and PRKCD are strong candidates for PTPN14 substrates.

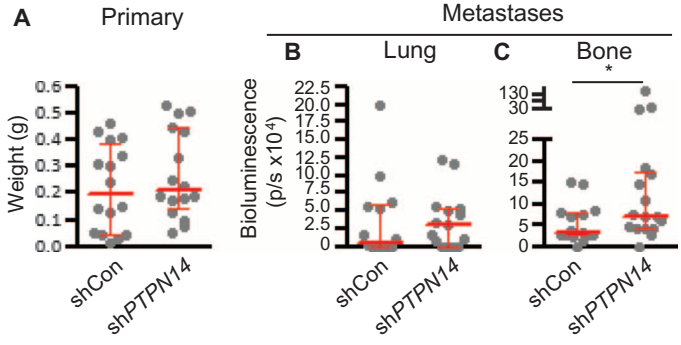

Fig. 3. PTPN14 depletion enhances metastatic potential by altering the cancer cell secretome. (**A** to **C**) Mass of primary tumors (A) and quantitation of metastases to the lung (B) or bone (C) from LM2-shCon xenografts 4 to 5 weeks after implantation. Each dot represents one mouse. *$P < 0.05$, Mann-Whitney *U* test.

Although none of the putative substrates identified have documented roles in regulating secretion, RIN1 [a Rab5 guanine nucleotide exchange factor implicated in receptor endocytosis (*33*–*36*)] and PRKCD [a functionally diverse Ser/Thr kinase (*37*–*40*)] have roles in receptor trafficking. We further investigated whether RIN1 and PRKCD are bona fide substrates using a number of other criteria. First, we demonstrated through coimmunoprecipitation that an active site competitive inhibitor, vanadate, could out-compete RIN1 or PRKCD for ST-PTPN14 binding (Fig. 4B). This observation also suggests that binding of RIN1 and PRKCD to PTPN14 may occur at the catalytic site of PTPN14 (*32*). We also validated the differential phosphoproteomic data: when PTPN14 was knocked down, the phosphorylation of both RIN1 and PRKCD was increased (Fig. 4, C and D). Finally, we were also able to show that PRKCD bound to ST-PTPN14 significantly better than it did to wild-type PTPN14, and that mutating Tyr^{374} of PRKCD to a nonphosphorylatable Phe abolished its enhanced binding to ST-PTPN14 (Fig. 4, E and F), strongly indicating that PRKCD bound to the active site of PTPN14 and that this binding was dependent on phosphorylation of Tyr^{374}.

Loss of PTPN14 catalytic activity or overexpression of candidate substrates RIN1 and PRKCD enhances IL-8 secretion

To ascertain whether the catalytic activity of PTPN14 was essential for suppressing the secretion of prometastatic factors, we overexpressed a catalytically inactive mutant of PTPN14 (C1121S) in MDA-MB-468 cells (fig. S8A) and saw increased secretion of IL-8, a representative cytokine from the pool of PTPN14-inhibited cytokines (Fig. 5A). This increase caused by loss of the catalytic function of PTPN14 phenocopied that caused by loss of total PTPN14 (Fig. 2C), whereas overexpression of wild-type PTPN14 suppressed IL-8 secretion (Figs. 2C and 5A and fig. S8A). Overexpressing the PTPN14 substrates RIN1 and PRKCD, which have known roles in receptor trafficking (*33*–*36*, *39*, *40*), in MDA-MB-468 cells increased IL-8 secretion, whereas overexpressing IRS1 (a putative substrate with no known role in protein trafficking) had no effect on IL-8 secretion (Fig. 5A and fig. S8A). In contrast, IL-8 secretion was suppressed by the addition of GF109203X, which predominantly inhibits classical and novel (including PRKCD) PRKCs, but not Go6976, an inhibitor of classical PRKCs (Fig. 5B). These data demonstrated novel roles for RIN1 and PRKCD in regulating the secretion of soluble proteins and, furthermore, indicated that the catalytic activity of PRKCD is most likely also essential for regulating secretion. That an inhibitor of PRKCD activity phenocopied the effect of PTPN14 overexpression further suggests that PTPN14 inhibits the activity of PRKCD to suppress secretion. This conclusion could potentially also extend to RIN1 because overexpression of RIN1 also increased IL-8 secretion (Fig. 5A).

PTPN14 and its substrates PRKCD and RIN1 regulate trafficking of receptors

Given the previously reported links between PRKCD and RIN1 and receptor trafficking (*33*–*36*, *39*, *40*), we tested whether PTPN14 and

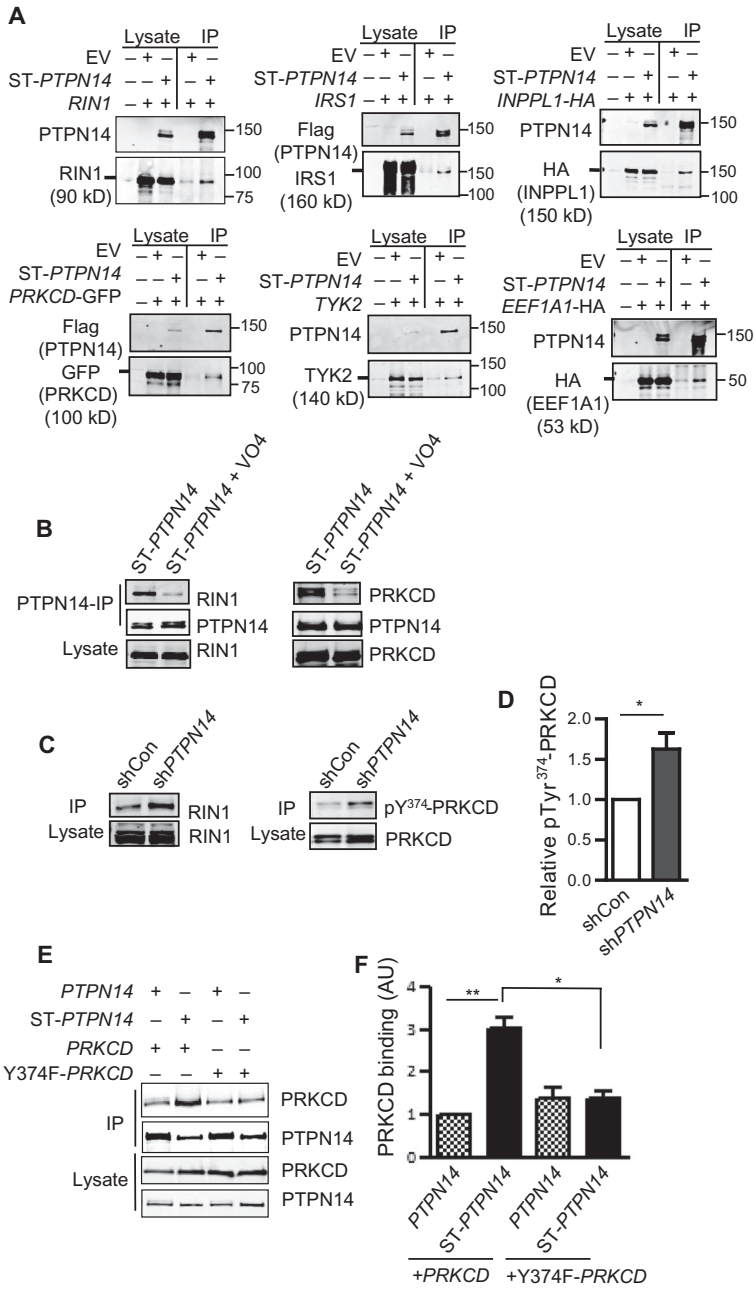

Fig. 4. Validation of candidate PTPN14 substrates identified by differential phosphoproteomics. (A) Immunoprecipitation with the Flag antibody in HEK 293T cells coexpressing Flag-tagged ST-PTPN14 and candidate PTPN14 substrates identified in the SILAC-MS screen. Blots are representative of at least three independent experiments. (B) Immunoprecipitations using the Flag antibody performed as in (A) in the presence or absence of 10 mM vanadate (VO_4) in HEK 293T cells coexpressing ST-PTPN14 and either RIN1 (left) or PRKCD (right). (C) Immunoprecipitations from MDA-MB-231 cells transfected with shCon or sh*PTPN14*, using either a pan-phosphotyrosine antibody (4G10; left) or a PRKCD antibody (right). Blots in (B) and (C) are representative of at least two experiments. (D) Abundance of phosphorylated Tyr^{374}-PRKCD ($pTyr^{374}$-PRKCD) relative to total PRKCD in the immunoprecipitates quantified from (C) and two additional experiments ($n = 3$). Data are means ± SD; $^*P < 0.05$, Student's *t* test. (E and F) Western blotting for proteins coimmunoprecipitated with the Flag antibody in HEK 293T cells that were transfected as indicated (E) and quantification of the amount of coimmunoprecipitated PRKCD relative to the amount of PTPN14 or ST-PTPN14 in each immunoprecipitate (F). AU, arbitrary units. Data are means ± SD from three blots; $^*P < 0.05$, $^{**}P < 0.01$, Student's *t* test.

its substrates affected the trafficking of receptors implicated in cancer progression. It has previously been shown that PTPN14 interacts with FLT4, a receptor critical for lymphatic development (*15*). We therefore investigated the relationship between PTPN14 and cell surface FLT4 in primary lymphatic endothelial cells. Knocking down PTPN14 increased the cell surface elaboration of FLT4, whereas knocking down PRKCD or RIN1 suppressed the cell surface elaboration of FLT4 (Fig. 5, C and D, and fig. S8B). Similar to its effect on protein secretion, PTPN14 suppressed the cell surface elaboration of FLT4, whereas its substrates PRKCD and RIN1 had the opposite effect. We also examined whether this effect extended to other receptors and other cell types by examining the effect of PTPN14 and RIN1 on EGFR (epidermal growth factor receptor) trafficking in the triple-negative breast cancer cell line BT549 using immunofluorescence to quantify cell surface EGFR (Fig. 5, E and F, and fig. S8C) as well as by biotinylation of cell surface proteins, isolation of the latter by Neutravidin pull-down, and detection by Western blotting (Fig. 5, G and H, fig. S8D). We found that wild-type PTPN14 suppressed the abundance of cell surface EGFR, but the catalytically inactive mutants, C1121S-PTPN14 and ST-PTPN14, acted as dominant negatives and promoted the cell surface presentation of EGFR, as did RIN1 overexpression (Fig. 5, F to H). The observation that the catalytically deficient mutants of PTPN14 acted as dominant negatives suggested that Tyr dephosphorylation by PTPN14 may be important in inhibiting the cell surface presentation of EGFR. In the case of RIN1, MS analysis revealed increased phosphorylation at Tyr^{36} in PTPN14-deficient cells compared to controls, suggesting that the phosphorylation state of RIN1 may determine the degree of EGFR present on the cell surface. Consistent with this hypothesis, overexpression of a nonphosphorylatable mutant of RIN1 (Y36F-RIN1) failed to promote cell surface EGFR presentation (Fig. 5H).

These data suggested that PTPN14 and its substrates PRKCD and RIN1 regulate one or more common pathways used for trafficking subsets of soluble proteins and receptors to the plasma membrane. Together, these data also indicated that the extent of phosphorylation at Tyr^{36} on RIN1, which is reduced in the presence of PTPN14, is instrumental in regulating such trafficking of cell surface receptors.

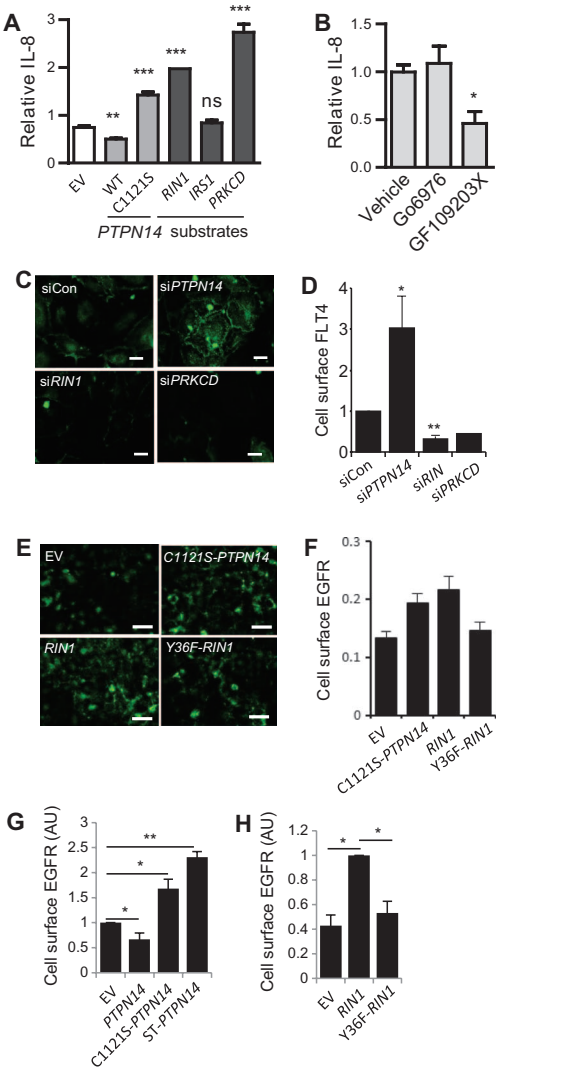

Fig. 5. PTPN14 and its candidate substrates alter secretion and receptor trafficking in a phosphorylation-dependent manner. (A and B) ELISA, normalized to number of cells, of the IL-8 abundance in CM from MDA-MB-468 cells that (A) expressed EV, wild-type (WT) PTPN14, or mutant PTPN14, or candidate PTPN14 substrates, or (B) were treated with vehicle, Go6976, or GF109203X. Data are means ± SD from at least three independent experiments; *$P < 0.05$ by one-way analysis of variance (ANOVA) with Bonferroni's multiple comparisons test; **$P < 0.01$, ***$P < 0.001$ by ANOVA with post hoc Tukey's test; ns, not significant. (C and D) Immunofluorescence (C) and quantification (D) of cell surface FLT4 on nonpermeabilized primary lymphatic endothelial cells transfected with the indicated small interfering RNA (siRNA). Scale bars, 0.02 mm. Data are means + SD of at least two transfections; *$P < 0.05$, **$P < 0.01$ by Student's t test. (E and F) Immunofluorescence (E) and quantification (F) of cell surface EGFR on nonpermeabilized, transfected BT549 cells. Scale bars, 0.05 mm. Data are means ± SD from a representative experiment, each with ≥300 cells. (G and H) Neutravidin-biotin analysis of cell surface EGFR on BT549 cells overexpressing either (G) WT or mutant PTPN14 or (H) WT or mutant RIN1. Data are means ± SD from three independent experiments; *$P < 0.05$, **$P < 0.01$, Student's t test.

High *RIN1* and *PRKCD* expression correlates with decreased survival in breast cancer patients

Because *PTPN14* is mutated in a number of cancers (*16*–*18*) and our data indicate that PTPN14 inhibited metastasis (Figs. 1, G to I, and 3), we analyzed whether its substrates *RIN1* and *PRKCD* also affect cancer progression using the The Cancer Genome Atlas (TCGA) breast cancer data set. We found that increased *RIN1* expression significantly correlated with decreased overall survival for all breast cancer patients analyzed, whereas increased *PRKCD* expression correlated with decreased overall survival of luminal A breast cancers (Fig. 6).

DISCUSSION

Our data demonstrated a direct effect of PTPN14 on cancer progression that is backed by clinical data showing that *PTPN14* expression is reduced in invasive compared to noninvasive breast cancer. We found that PTPN14 acts to reduce the secretion of a suite of prometastatic factors to suppress metastasis, most likely through regulating the activities of its substrates, PRKCD and RIN1. In so doing, we have uncovered novel functions for PRKCD and RIN1 that, although previously shown to function in receptor trafficking, had no known roles in regulating trafficking of soluble proteins. Of particular interest then is our finding that high expression of the PTPN14 substrates RIN1 and PRKCD correlated with poor patient survival in breast cancer, which concurs with previously published reports that PRKCD negatively correlates with survival in breast cancer patients (*41*) and RIN1 negatively correlates with survival in melanoma (*42*), gastric adenocarcinoma (*43*), bladder urothelial carcinoma (*44*), and non–small cell lung cancer (*45*). Recognizing that the trafficking of prometastatic factors and growth factor receptors is inhibited by PTPN14, and that it is promoted by PRKCD and RIN1, our findings reveal potential strategies for simultaneously reducing the mobilization of soluble factors and cell surface receptors that promote tumor cell growth and survival.

The role that tyrosine phosphorylation pathways play in regulating trafficking processes is not well characterized. Our mass spectrometry data suggested that PTPN14 dephosphorylates PRKCD at Tyr^{374} and RIN1 at Tyr^{36}. How the phosphorylation of Tyr^{374} affects PRKCD activity and which tyrosine kinase phosphorylates it is unknown, but it is noteworthy that this tyrosine is just two amino acids away from the ATP (adenosine triphosphate)–binding site. Recent studies indicate that PRKCD regulates the balance between targeting receptors for degradation versus recycling to the cell surface (*40*), and it will be of interest to determine whether

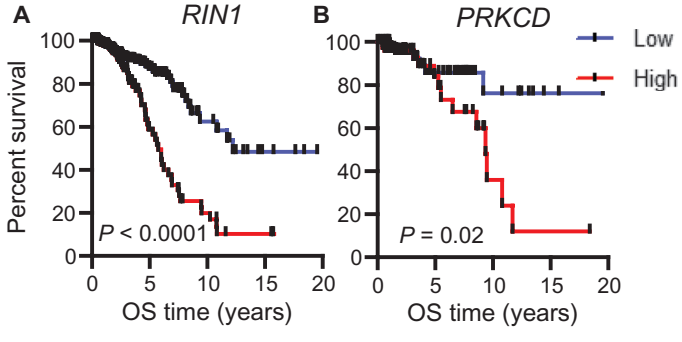

Fig. 6. Decreased survival of breast cancer patients with elevated RIN1 and PRKCD. (A and B) Kaplan-Meier analysis of breast cancer samples from TCGA showing overall survival (OS) over time for (A) RIN1 in all breast cancer patients (n = 689 patients) or (B) PRKCD in luminal A patients (n = 175 patients).

Tyr^{374} phosphorylation shifts the balance to recycling. Because cells with higher PRKCD also had higher cell surface FLT4, it suggests that this could indeed be due to higher overall PRKCD activity tipping the balance toward receptor recycling. Tyr^{36} on RIN1 is phosphorylated by the Abl tyrosine kinase, which in turn creates a binding site for Abl through its SH2 domain and thereby relieves autoinhibition (*46*, *47*) of its kinase activity. In the same work (*46*), the authors showed that phosphorylation of Tyr^{36} stabilizes the RIN1 interaction with Abl and promotes the activation of Abl kinase, which is known to promote cancer cell motility and invasion. It is therefore possible that a strong decrease in PTPN14 phosphatase activity could promote an invasive phenotype by signaling via RIN1 Tyr^{36} phosphorylation to Abl. Studies on the interaction of FLT4 with RIN1 have not been reported, and the role of RIN1 in receptor trafficking is best understood with EGFR. A consequence of stable binding of Abl to RIN1 is the inhibition of macropinocytosis and the clathrin-independent internalization of receptors and their delivery to the lysosome for degradation (*36*). Thus, it has been proposed that it is the balance between the phospho-Tyr^{36}–independent RIN1-Rab5 interaction, which leads to EGFR down-regulation, and the phospho-Tyr^{36}–dependent RIN1-Abl interaction, which inhibits macropinocytosis, that determines the net amount of receptors present on the cell surface (*36*). Our data would suggest that PTPN14 inhibits the RIN1-Abl interaction by keeping Tyr^{36} dephosphorylated, thereby maintaining a steady rate of macropinocytosis. Overexpressing RIN1 in the absence of growth factor stimulation increases the total amount of phosphoTyr^{36}-RIN1 (*36*), and this could shift the balance toward inhibiting macropinocytosis without perturbing the Rab5-mediated functions and thereby leading to an overall increase in cell surface receptor presentation. On the basis of these data, we propose a model whereby PTPN14 regulates receptor trafficking through PRKCD and RIN1 (Fig. 7). Because both the secretion of soluble proteins and the cell surface presentation of receptors appear to be inhibited by PTPN14, we propose that the suite of soluble proteins whose secretion is inhibited by PTPN14 must traffic through the endosomal compartments controlled by PRKCD and RIN1 during export.

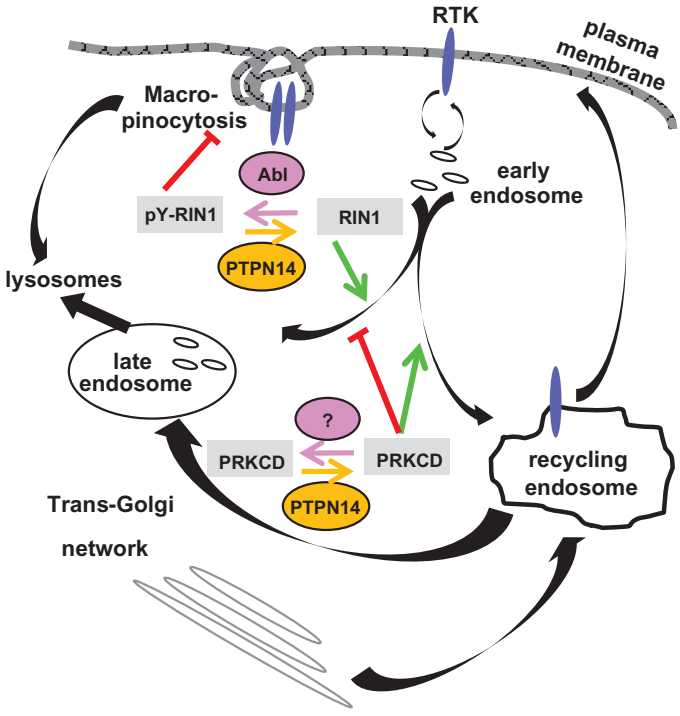

Fig. 7. Regulation of receptor trafficking by PTPN14 and its substrates. Model showing potential mechanism through which PTPN14 and its substrates, PRKCD and RIN1, regulate receptor trafficking, combining the data reported in this study with published data on PRKCD and RIN1 (*36*, *40*, *52*). Cell surface receptors internalized into early endosomes can be recycled through the recycling endosomes or be directed to lysosomes for degradation. PRKCD when activated can increase cell surface receptor numbers by promoting recycling or inhibiting trafficking to lysosome or both. We propose that PTPN14 regulates this trafficking by keeping Tyr^{374} on PRKCD dephosphorylated to decrease its activity and thereby decrease the cell surface presentation of receptors. Receptors can also be internalized by macropinocytosis followed by degradation in the lysosomes, which may be inhibited when RIN1 is phosphorylated on Tyr^{36}. PTPN14 dephosphorylates Tyr^{36} to de-repress macropinocytosis, leading to decreased cell surface receptor numbers.

MATERIALS AND METHODS

Plasmids, transfection, and generation of stable cell lines

The N-terminal Flag-tagged PTPN14 expression plasmid has been previously described (*19*). The C1121S mutation was introduced into an existing Flag-tagged PTPN14 D1079A mutant construct (*19*) using site-directed mutagenesis to generate the substrate-trapping mutant of PTPN14. RIN1 (SC 122674), IRS1 (SC 124032), and TYK2 (SC 128128) plasmids were purchased from OriGene. Hemagglutinin (HA)–tagged INPPL1 plasmid was a gift from C. Mitchell, HA-tagged eEF1A1 plasmid was a gift from S. Pitson, green fluorescent protein (GFP)–tagged PRKCD was a gift from J.-W. Soh, and PRKCD was a gift from C. Larsson.

To generate PTPN14-knockdown cell lines, MDA-MB-231 cells or a derivative [(MDA-MB-231 LM2 (*28*)] were transduced with the pLMP retroviral vector expressing an shRNA targeting human *PTPN14* (sh*PTPN14*) or a nontargeting control shRNA (shCon). After selection in puromycin, individual clones were screened for amount of PTPN14 protein, and pools of four individual clones were used for the analyses. PTPN14-overexpressing MDA-MB-468 cells were generated by transfecting adherent MDA-MB-468 cells with N-terminal Flag-tagged human PTPN14 complementary DNA (cDNA) (*19*) in pEF-IRES-puro vector using FuGene HD transfection reagent (Roche). After selection, three individual clones were used for subsequent studies.

Analysis of primary human breast cancer samples

PTPN14 expression in primary human breast cancers was determined as previously described (*26*). Briefly, formalin-fixed, paraffin-embedded (FFPE) de-identified sections from DCIS or invasive ductal breast cancer samples were obtained from the Department of Tissue Pathology at SA Pathology. Access to patient tumor samples was approved by the appropriate institutional human ethics review boards. Sections were H&E-stained, and regions that contained primarily tumor cells were marked for further analysis. Using duplicate unstained sections, marked areas of the tumor were scraped into tubes where total RNA was isolated using an miRNeasy FFPE Kit (Qiagen). cDNA was specifically primed, and then real-time PCR analysis for mRNA was performed using TaqMan assays (Applied Biosystems); results were expressed relative to GAPDH. Samples were obtained from one to two distinct regions from each patient specimen. Each was separately assayed, and the triplicate values were averaged and then treated as individual data points.

3D organotypic invasion assay

Organotypic assays were performed as described previously (*29*). Briefly, collagen I was extracted under acidic conditions from rat tails and polymerized in

the presence of about 3×10^4 fibroblasts. Detached collagen discs (35 mm in diameter) were allowed to contract to a diameter of less than 15 mm when 1×10^5 cells of interest were seeded on top of each submerged matrix. After 4 days, these matrices were transferred to metal grids and exposed to an air-liquid interface to trigger invasion. MDA-MB-231 (LM2) cells were allowed to invade for 10 days, whereas MDA-MB-231 cells were allowed to invade for 12 days. All incubations were performed in Dulbecco's modified Eagle's medium (DMEM) + 10% serum + 1% penicillin and streptomycin at 37°C and 5% CO_2. Subsequently, matrices were fixed in formalin and processed for H&E staining and Ki67 immunohistochemistry. Representative pictures were taken with a Leica DMI 6000 at ×20 magnification. Cell invasion was quantified by normalizing the number of cells that invaded into the matrix to the total number of cells (total number = invaded cells + cells on top of the matrix with immediate contact to the collagen). Cell proliferation was quantified by normalizing the number of $Ki67^+$ cells to the total number of cells.

Mouse xenograft orthotopic metastasis model

The mouse orthotopic (mammary fat pad) tumor metastasis model was essentially as described (*48*), except that MDA-MB-231 LM2 cells expressing *PTPN14* or control shRNAs were used. For the conditioned medium experiments, conditioned medium was injected intraperitoneally daily, beginning 3 days before engraftment of the shCon cells into mammary fat pad.

Cytokine antibody arrays

Individual clones from each of 468-EV (three clones), 468-PTPN14 (three clones), 231-shCon (four clones), or 231-sh*PTPN14* (four clones) were seeded at 2×10^5 cells per well in 24-well plates. After 24 hours, cells were washed and placed into low-serum medium [DMEM with 0.1% fetal bovine serum (FBS) and 1× nonessential amino acids (NEAAs)], and equal amounts of conditioned medium collected from each clone were pooled. Conditioned medium was centrifuged at 1000*g* for 15 min at 4°C, and the supernatant was collected for use. Each pool of conditioned media was analyzed for relative cytokine content, using RayBio Human Cytokine Antibody Array C Series 1000 membranes (RayBiotech) according to the manufacturer's instructions. Multi Gauge software (Fujifilm) was used for quantitation of signal intensities for each hybridization position on the array membranes. Raw data were collected as total pixels per position, with two hybridization positions for each cytokine, and normalized using a normalization factor derived for each membrane by calculating the average pixel value across six positive control positions. Normalized values were averaged to determine fold change in cytokine abundance with PTPN14 overexpression (468-PTPN14/468-EV) or *PTPN14* knockdown (231-sh*PTPN14*/231-shCon).

Bio-Plex bead suspension analysis

VEGF, IL-6, and IL-8 present in the conditioned medium of PTPN14-overexpressing or PTPN14-knockdown cell lines were also measured by a multiplex bead antibody array, using Bio-Plex Pro Human Cytokine Panel (Bio-Rad) according to the manufacturer's instructions.

Stable isotope labeling with amino acids in cell culture

shCon and sh*PTPN14* MDA-MB-231 cells were cultured in DMEM supplemented with puromycin (1 μg/ml), 10% dialyzed FBS (Sigma-Aldrich), and either "light" ($C^{12}N^{14}$) or "heavy" ($C^{13}N^{15}$) arginine and lysine (0.199 and 0.798 mM, respectively) (Cambridge Isotopes). Cells were labeled over the course of five doublings, using two biological replicates of each cell line with inversed labeling between biological replicates. Complete heavy isotope incorporation was confirmed by mass spectrometry, and no heavy proline conversion was detected.

Phosphotyrosine peptide immunoprecipitation

Subconfluent cells were collected in lysis buffer (8 M urea, 20 mM Hepes, 2.5 mM sodium pyrophosphate, 1 mM β-glycerophosphate, 1 mM sodium orthovanadate, 1 mM EDTA, and 1 mM TCEP, pH 8.0) and cleared by sonication and centrifugation. Twenty milligrams of each lysate (heavy/light) was mixed, diluted to a final concentration of 1 M urea with 20 mM Hepes, and digested with trypsin at room temperature overnight. Peptides were then desalted and concentrated using C_{18} Sep-Pak columns (Waters) and lyophilized. Phosphotyrosine peptides were immunoprecipitated using a PhosphoScan Kit (Cell Signaling Technology) with pY100 antibodies as previously described (*49*). Unbound sample flow-through from the pY100 antibodies was further immunoprecipitated with pY20 antibodies (BD Scientific) overnight at 4°C. Immunoprecipitated peptides were dried using a vacuum centrifuge and stored at −80°C before analysis by nano-LC–MS/MS.

Nano-LC–MS/MS data acquisition

Phosphotyrosine peptides were resuspended in 15 μl of MS buffer containing 1% formic acid, 2% acetonitrile (ACN), and 0.05% heptafluorobutyric acid and subjected to nano-LC–MS/MS. Peptides were separated by nano-LC using an Ultimate 3000 HPLC and autosampler system (Dionex). Samples were concentrated and desalted onto a micro C_{18} pre-column (500 μm x 2 mm, Michrom Bioresources) with H_2O/ACN (98:2, 0.05% trifluoroacetic acid) at 15 μl/min for 4 min. The pre-column was then switched on-line with a nano-C_{18} column (75 μm x ~10 cm, 5 μm, 200 Å Magic, Michrom), and the reverse-phase nano-eluent was subjected to positive nano-flow electrospray analysis in an information-dependent acquisition mode (IDA) (250 nl/min over 30 min). Mass spectra were acquired on an Orbitrap Velos mass spectrometer (Thermo Electron). In IDA mode, survey scans in the range *m/z* (mass/charge ratio) 350 to 1750 were acquired with lockmass enabled. Up to the 15 most abundant ions (>5000 counts) with charge states >+2 were sequentially isolated and further subjected to MS/MS fragmentation within the linear ion trap using collisionally induced dissociation. MS/MS spectra were accumulated with an activation time of 30 ms at a target value of 30,000 ions and a resolution of 60,000. *m/z* ratios selected for MS/MS were dynamically excluded for 30 s.

Protein identification and quantitation

The nano-LC–MS/MS raw files were processed with MaxQuant software (version 1.1.1.36), which uses the Andromeda algorithm for data processing, database searching, and protein identification (*50*). Extracted peak lists were searched against the UniProtKB/Swiss-Prot *Homo sapiens* database (version 2010_10) containing 35,052 entries (including common contaminants) and a proportionally sized decoy database for false discovery rate (FDR) generation. The following search parameters were selected: fixed cysteine carbamidomethylation modification, variable methionine oxidation modification, variable protein N-acetylation, and variable phosphorylation of serine, threonine, and tyrosine; a minimum peptide length of six amino acids and up to two missed cleavages were allowed. For SILAC quantitation, SILAC multiplicity was set to 2 and heavy +10-dalton Arg, +8-dalton Lys were selected. The initial first search mass tolerance was 20 ppm for precursor ions and 0.5 dalton for fragment ions; the "match between runs" (with default settings) and "re-quantify" options were enabled. The FDR was limited to 1% for both protein and peptide identifications.

Selection criteria and data filtering

Strict criteria were used to select high-quality phosphotyrosine peptides for subsequent quantitative analysis: (i) phosphotyrosine peptides must be identified with an FDR of <1% and an Andromeda score >60, (ii) phosphotyrosine peptides must contain a phosphorylated tyrosine residue with a site localization probability confidence ≥0.75, and (iii) phosphotyrosine

peptides must be identified from both technical and biological replicates, resulting in a minimum of four quantified SILAC pairs. Phosphotyrosine peptides were considered unique on the basis of amino acid sequence and phosphorylation site.

Quantitative analysis of SILAC ratios

After selection filtering, SILAC ratios between heavy and light isotope-labeled phosphotyrosine peptides were determined. To assess the effects of PTPN14 knockdown, the ratios of phosphopeptides were obtained by comparing sh*PTPN14* to shCon samples. For samples that were inversely labeled, 1/ratio was used. The ratios were converted to fold changes by calculating their deviation from 1 (for example, a ratio of 0.5 is equal to −2-fold change, and a ratio of 2.0 is equal to +2-fold change). Phosphotyrosine peptides that exhibited a fold change of ±1.2 were considered to be differentially abundant.

Differential phosphoproteomic screen

Briefly, PTPN14-knockdown and control cells were labeled with heavy and light amino acid isotopes, respectively, and after mixing of cell lysates and tryptic digestion, phosphotyrosine-containing tryptic peptides were isolated by serial immunoprecipitation with pY100 and pY20 anti-phosphotyrosine antibodies. Analysis by nano-LC–MS/MS was then undertaken, with two technical replicates. A second experiment was also performed with the isotope labels switched, providing a biological replicate experiment.

Three hundred twenty-two nonredundant phosphotyrosine sites were identified at an FDR of <1%. After application of stringent selection criteria (see above), 278 high-confidence nonredundant phosphotyrosine sites that exhibited a phosphorylation site localization probability of ≥0.75 and an Andromeda score >60 remained for further analysis. A high degree of overlap was observed between technical replicates for these high-confidence phosphotyrosine sites from both biological replicates when using either pY100 or pY20 antibodies (fig. S9, A and D). Correlation coefficients (R^2) were calculated for these technical replicates on the basis of their phosphotyrosine site SILAC ratios (fig. S9, B and D). R^2 values between 0.80 and 0.87 were observed, demonstrating a high degree of reproducibility between replicate MS runs. Of the 278 high-confidence phosphotyrosine sites identified, 111 unique phosphotyrosine sites were consistently identified in both technical and biological replicates from pY100 immunoprecipitations, and 68 were identified from pY20 immunoprecipitations. These high-confidence and consistently observed phosphotyrosine sites were filtered to remove duplicate entries and peptide differences of <1.2-fold in both biological replicates. A significant correlation of SILAC ratios was observed between biological replicate experiments for the 29 phosphosites displaying altered phosphorylation in both experiments ($R^2 = 0.57$, $P < 0.0001$; fig. S9E), indicating reproducibility between independent experiments.

Coimmunoprecipitation

HEK 293T cells (1×10^6) were transfected with 2 μg of candidate substrate plasmid and 2 μg of pCDNA3 (EV) or ST-PTPN14, using Lipofectamine 2000 (Invitrogen) according to the manufacturer's instructions. Twenty-four hours after transfection, cell pellets were washed in cold phosphate-buffered saline (PBS) and lysed in 1 ml of lysis buffer [20 mM tris-Cl (pH 7.4), 137 mM NaCl, 10% glycerol, 0.5 to 1% NP40], supplemented with 1× "complete" mini EDTA-free protease inhibitors (Roche), 10 mM NaF, and 10 mM β-glycerophosphate, for 15 min at 4°C and centrifuged 16,000*g*, 10 min at 4°C to remove cell debris. Lysate (25 μl) was saved for analysis, and the remainder was immunoprecipitated with 2 μg of antibody recognizing the Flag epitope (M2; Sigma) for 2 hours at 4°C, followed by 1-hour capture with protein G–Sepharose beads [preblocked overnight at 4°C in 50 mM tris-Cl, 200 mM ethanolamine, 1% Tween 20 (pH 10.6) and washed with PBS before use]. Beads were collected by centrifugation at 16,000*g* for 20 to 30 s and washed twice in 1 ml of 1% NP40 lysis buffer and once in 1 ml of 0.5% NP40 lysis buffer; immunoprecipitated proteins were eluted in 40 μl of 2× SDS load buffer [100 mM tris-Cl (pH 6.8), 4% SDS, 20% glycerol, 0.005% bromophenol blue] by boiling the samples for 5 min at 95°C before analysis by Western blotting.

Western blotting

For Western blotting, antibodies were used at the following concentrations: rabbit antibody against PTPN14 (*19*) at 1:1000; mouse antibody against the Flag epitope (M2, Sigma) at 1:2000; goat antibody against RIN1 (sc-1971, Santa Cruz Biotechnology) at 1:1000; rabbit antibody against IRS1 (#2382, Cell Signaling Technology) at 1:1000; mouse antibody against INPPL1 (sc-166641, Santa Cruz Biotechnology) at 1:200; mouse antibody against TYK2 (#610173, BD Transduction Laboratories) at 1:1000; mouse antibody against eEF1A (#05-235, Millipore) at 1:1000; rabbit antibody against GFP (sc-8334, Santa Cruz Biotechnology) at 1:1000; rabbit antibody against HA (#3724, Cell Signaling Technology) at 1:1000; mouse antibody against tubulin (ab7291, Abcam) at 1:5000; goat antibody against actin (sc-1616, Santa Cruz Biotechnology) at 1:5000.

Generation of pTyr^{374}-PRKCD antibody

An antibody specific to phosphorylated Tyr^{374} of PRKCD (pTyr^{374}-PRKCD) was raised using a phosphopeptide encompassing Tyr^{374} of PRKCD (H-CKGRGEpYFAIKAL-NH_2), where pY is phosphotyrosine (Mimotopes). The phospho-Tyr^{374}-PRKCD peptide was coupled to keyhole limpet hemocyanin and injected into New Zealand White rabbits. Test bleeds for immunoreactivity against nonphosphorylated Tyr^{374}-PRKCD or phospho-Tyr^{374}-PRKCD peptides using a dot blot format indicated that the immunoreactive serum was highly selective for the phospho-Tyr^{374}-PRKCD peptides.

IL-8 ELISA

MDA-MB-468 cells were seeded at 1.8 x 10^5 to 2.0 x 10^5 cells per well in 24-well plates and transfected with either an EV (pcDNA3), wild-type PTPN14, C1121S-PTPN14, RIN1, IRS1, or PRKCD, using Xtreme-GENE HP (Roche) according to the manufacturer's instructions, or treated with the protein kinase C inhibitor Go6976 [31 nM, 5× IC_{50} (half maximal inhibitory concentration)] or GF109203X (1.05 μM, 5× IC_{50}) (Tocris). After 24 hours, cells were washed and then incubated in low-serum medium (DMEM with 0.1% FBS and 1× NEAAs) for 24 hours, and then the conditioned media were collected. The remaining cells were lysed in Triton X-100 lysis buffer [150 mM NaCl, 1% Triton X-100, 50 mM tris (pH 8)], and lysates were used for evaluating the overexpression of transfected proteins by Western blot analysis. IL-8 ELISA was performed using RayBio IL-8 ELISA kit according to the manufacturer's instructions.

Staining for cell surface receptor FLT4

Primary human lymphatic endothelial cells (HMVECdLyAd) (Lonza) were seeded on fibronectin-coated chamber slides (Nunc-Thermo Scientific) at 1.4×10^4 cells per well. Cells were transfected in suspension with siCon, si*PTPN14*, si*RIN1*, or si*PRKCD* (Ambion), using RNAiMAX (Invitrogen) according to the manufacturer's instructions. After 48 hours, cells were starved in low-serum medium (EBM2 basal with 0.1% FBS) (Lonza) for 4 hours, followed by incubation with the antibody FLT4-ECD (extracellular domain–specific; BD Biosciences) for 1 hour at 4°C. Cells were then washed three times with ice-cold PBS and fixed in 4% paraformaldehyde (PFA) for 10 min. Cells were then washed three times with tris-buffered saline (TBS), incubated with block buffer (TBS, 2% bovine serum albumin) for 1 hour at room temperature, incubated with Alexa 488–conjugated antibody against mouse immunoglobulin (Life Technologies), washed three

times in immunofluorescence wash buffer (TBS, 0.1% Triton X-100), and mounted using ProLong Gold with 4′,6-diamidino-2-phenylindole (DAPI) (Molecular Probes).

EGFR cell surface staining

BT549 cells were seeded on fibronectin-coated chamber slides (Nunc-Thermo Scientific) at 5×10^4 cells per well. Cells were transfected with an EV, C1121S-PTPN14, RIN1, or Y36F-RIN1, using Lipofectamine 2000 (Invitrogen) according to the manufacturer's instructions. After 24 hours, cells were starved in low-serum medium (DMEM with 0.1% FBS) for 24 hours and then incubated with an antibody recognizing the extracellular domain of EGFR (Thermo Scientific) for 1 hour at 4°C. Cells were washed three times with ice-cold PBS, fixed in 4% PFA for 10 min, and then stained with Alexa 488–conjugated secondary antibody and mounted as described above.

Quantifying cell surface receptors after immunofluorescence staining

Slides were imaged on an LSM 700 confocal scanning microscope (Zeiss), and image analysis with Fiji software (*51*) was done to quantify the amount of fluorescence on the cell surface as described below. Acquired images were collated into a stack and converted to 8-bit images. A threshold was applied to the entire stack to highlight cell surface receptor staining. Percent cell surface staining under each condition was determined using percent area function under the "analyze particles" option. This provided the percent area per field of view. Cell number in each field of view was determined by counting DAPI-stained nuclei by applying image threshold function to highlight the nuclei and perform a count using the "analyze particles" option excluding objects smaller than 5 μm^2. The percent area per field of view was divided by total cell number per field of view. Mean percent area per cell was calculated for all the fields of view per treatment condition.

Quantifying cell surface EGFR by biotinylation of cell surface proteins

BT549 cells were seeded on 12-well plates at 2×10^5 cells per well. Cells were transfected with an EV, wild-type PTPN14, C1121S-PTPN14, ST-PTPN14, RIN1, or Y36F-RIN1, using Lipofectamine 2000 (Invitrogen) according to the manufacturer's instructions. After 24 hours, cells were starved in low-serum medium (DMEM with 0.1% FBS) for 24 hours. Cells were washed three times with PBS (pH 8) and then incubated with 0.4 mM EZ-Link-Sulfo-NHS-SS-Biotin (Thermo Scientific) in PBS (pH 8) for 1 hour at 4°C. Cells were then washed three times with ice-cold PBS (pH 8); scraped into 1 ml of lysis buffer [20 mM tris-Cl (pH 7.4), 137 mM NaCl, 10% glycerol, 0.5 to 1% NP40] supplemented with 1× complete mini EDTA-free protease inhibitors (Roche), 10 mM NaF, and 10 mM β-glycerophosphate; lysed for 15 min at 4°C; and centrifuged at 16,000*g* for 10 min at 4°C to remove cell debris. Lysate (25 μl) was saved for analysis, and the remainder was immunoprecipitated with 40 μl of Neutravidin agarose beads recognizing biotinylated proteins (Pierce Biotechnology) for 1 hour at 4°C. Beads were collected by centrifugation at 16,000*g* for 20 to 30 s and washed three times in 1 ml of 1% NP40 lysis buffer. Immunoprecipitated proteins were eluted in 40 μl of 2× SDS load buffer [100 mM tris-Cl (pH 6.8), 4% SDS, and 20% glycerol].

SUPPLEMENTARY MATERIALS

www.sciencesignaling.org/cgi/content/full/8/364/ra18/DC1

Fig. S1. PTPN14 knockdown promotes invasiveness in MDA-MB-231 cells.
Fig. S2. PTPN14 promotes the secretion of TGFβ in human breast cancer cell lines.
Fig. S3. Relative cytokine abundance in conditioned media from breast cancer cells after PTPN14 overexpression or knockdown.
Fig. S4. Relative abundance of cytokine mRNA transcripts in breast cancer cells after PTPN14 overexpression or knockdown.
Fig. S5. Schematic of the injection protocol used to test the effect of conditioned medium on the growth and metastasis of breast cancer cells in mice.
Fig. S6. Identification of PTPN14 substrates by differential phosphoproteomics.
Fig. S7. Total protein abundance of candidate PTPN14 substrates is unaffected by PTPN14 knockdown.
Fig. S8. Western blot analyses to ascertain overexpression or knockdown efficiencies.
Fig. S9. Correlation between technical replicate SILAC-MS experiments.
Table S1. List of candidate PTPN14 (Pez) substrates from SILAC-MS screen.
References (*53*–*62*)

REFERENCES AND NOTES

1. D. Hanahan, R. A. Weinberg, Hallmarks of cancer: The next generation. *Cell* **144**, 646–674 (2011).
2. H. Peinado, S. Lavotshkin, D. Lyden, The secreted factors responsible for pre-metastatic niche formation: Old sayings and new thoughts. *Semin. Cancer Biol.* **21**, 139–146 (2011).
3. R. N. Kaplan, R. D. Riba, S. Zacharoulis, A. H. Bramley, L. Vincent, C. Costa, D. D. MacDonald, D. K. Jin, K. Shido, S. A. Kerns, Z. Zhu, D. Hicklin, Y. Wu, J. L. Port, N. Altorki, E. R. Port, D. Ruggero, S. V. Shmelkov, K. K. Jensen, S. Rafii, D. Lyden, VEGFR1-positive haematopoietic bone marrow progenitors initiate the pre-metastatic niche. *Nature* **438**, 820–827 (2005).
4. H. Peinado, M. Alečković, S. Lavotshkin, I. Matei, B. Costa-Silva, G. Moreno-Bueno, M. Hergueta-Redondo, C. Williams, G. García-Santos, C. Ghajar, A. Nitadori-Hoshino, C. Hoffman, K. Badal, B. A. Garcia, M. K. Callahan, J. Yuan, V. R. Martins, J. Skog, R. N. Kaplan, M. S. Brady, J. D. Wolchok, P. B. Chapman, Y. Kang, J. Bromberg, D. Lyden, Melanoma exosomes educate bone marrow progenitor cells toward a pro-metastatic phenotype through MET. *Nat. Med.* **18**, 883–891 (2012).
5. M. Makridakis, A. Vlahou, Secretome proteomics for discovery of cancer biomarkers. *J. Proteomics* **73**, 2291–2305 (2010).
6. L. Sepiashvili, A. Hui, V. Ignatchenko, W. Shi, S. Su, W. Xu, S. H. Huang, B. O'Sullivan, J. Waldron, J. C. Irish, B. Perez-Ordonez, F. F. Liu, T. Kislinger, Potentially novel candidate biomarkers for head and neck squamous cell carcinoma identified using an integrated cell line-based discovery strategy. *Mol. Cell. Proteomics* **11**, 1404–1415 (2012).
7. D. Hanahan, L. M. Coussens, Accessories to the crime: Functions of cells recruited to the tumor microenvironment. *Cancer Cell* **21**, 309–322 (2012).
8. G. Pocsfalvi, G. Votta, A. De Vincenzo, I. Fiume, D. A. Raj, G. Marra, M. P. Stoppelli, I. Iaccarino, Analysis of secretome changes uncovers an autocrine/paracrine component in the modulation of cell proliferation and motility by c-Myc. *J. Proteome Res.* **10**, 5326–5337 (2011).
9. P. M. Neilsen, J. E. Noll, R. J. Suetani, R. B. Schulz, F. Al-Ejeh, A. Evdokiou, D. P. Lane, D. F. Callen, Mutant p53 uses p63 as a molecular chaperone to alter gene expression and induce a pro-invasive secretome. *Oncotarget* **2**, 1203–1217 (2011).
10. A. Bronisz, J. Godlewski, J. A. Wallace, A. S. Merchant, M. O. Nowicki, H. Mathsyaraja, R. Srinivasan, A. J. Trimboli, C. K. Martin, F. Li, L. Yu, S. A. Fernandez, T. Pécot, T. J. Rosol, S. Cory, M. Hallett, M. Park, M. G. Piper, C. B. Marsh, L. D. Yee, R. E. Jimenez, G. Nuovo, S. E. Lawler, E. A. Chiocca, G. Leone, M. C. Ostrowski, Reprogramming of the tumour microenvironment by stromal PTEN-regulated miR-320. *Nat. Cell Biol.* **14**, 159–167 (2012).
11. Y. Khew-Goodall, G. J. Goodall, Stromal miR-320 keeps an oncogenic secretome in check. *Nat. Cell Biol.* **14**, 124–125 (2012).
12. A. L. Smith, P. J. Mitchell, J. Shipley, B. A. Gusterson, M. V. Rogers, M. R. Crompton, *Pez*: A novel human cDNA encoding protein tyrosine phosphatase- and ezrin-like domains. *Biochem. Biophys. Res. Commun.* **209**, 959–965 (1995).
13. L. Wyatt, C. Wadham, L. A. Crocker, M. Lardelli, Y. Khew-Goodall, The protein tyrosine phosphatase Pez regulates TGFβ, epithelial–mesenchymal transition, and organ development. *J. Cell Biol.* **178**, 1223–1235 (2007).
14. I. Poernbacher, R. Baumgartner, S. K. Marada, K. Edwards, H. Stocker, *Drosophila* Pez acts in Hippo signaling to restrict intestinal stem cell proliferation. *Curr. Biol.* **22**, 389–396 (2012).
15. A. C. Au, P. A. Hernandez, E. Lieber, A. M. Nadroo, Y. M. Shen, K. A. Kelley, B. D. Gelb, G. A. Diaz, Protein tyrosine phosphatase PTPN14 is a regulator of lymphatic function and choanal development in humans. *Am. J. Hum. Genet.* **87**, 436–444 (2010).
16. Z. Wang, D. Shen, D. W. Parsons, A. Bardelli, J. Sager, S. Szabo, J. Ptak, N. Silliman, B. A. Peters, M. S. van der Heijden, G. Parmigiani, H. Yan, T. L. Wang, G. Riggins, S. M. Powell, J. K. Willson, S. Markowitz, K. W. Kinzler, B. Vogelstein, V. E. Velculescu, Mutational analysis of the tyrosine phosphatome in colorectal cancers. *Science* **304**, 1164–1166 (2004).
17. T. Sjöblom, S. Jones, L. D. Wood, D. W. Parsons, J. Lin, T. D. Barber, D. Mandelker, R. J. Leary, J. Ptak, N. Silliman, S. Szabo, P. Buckhaults, C. Farrell, P. Meeh, S. D. Markowitz, J. Willis, D. Dawson, J. K. Willson, A. F. Gazdar, J. Hartigan, L. Wu, C. Liu, G. Parmigiani, B. H. Park, K. E. Bachman, N. Papadopoulos, B. Vogelstein, K. W. Kinzler, V. E. Velculescu, The consensus coding sequences of human breast and colorectal cancers. *Science* **314**, 268–274 (2006).
18. M. Li, H. Zhao, X. Zhang, L. D. Wood, R. A. Anders, M. A. Choti, T. M. Pawlik, H. D. Daniel, R. Kannangai, G. J. A. Offerhaus, V. E. Velculescu, L. Wang, S. Zhou,B. Vogelstein,

R. H. Hruban, N. Papadopoulos, J. Cai, M. S. Torbenson, K. W. Kinzler, Inactivating mutations of the chromatin remodeling gene *ARID2* in hepatocellular carcinoma. *Nat. Genet.* **43**, 828–829 (2011).
19. C. Wadham, J. R. Gamble, M. A. Vadas, Y. Khew-Goodall, The protein tyrosine phosphatase Pez is a major phosphatase of adherens junctions and dephosphorylates β-catenin. *Mol. Biol. Cell* **14**, 2520–2529 (2003).
20. X. Liu, N. Yang, S. A. Figel, K. E. Wilson, C. D. Morrison, I. H. Gelman, J. Zhang, PTPN14 interacts with and negatively regulates the oncogenic function of YAP. *Oncogene* **32**, 1266–1273 (2013).
21. P. Zhang, A. Guo, A. Possemato, C. Wang, L. Beard, C. Carlin, S. D. Markowitz, R. D. Polakiewicz, Z. Wang, Identification and functional characterization of p130Cas as a substrate of protein tyrosine phosphatase nonreceptor 14. *Oncogene* **32**, 2087–2095 (2013).
22. M. Ogata, T. Takada, Y. Mori, M. Oh-hora, Y. Uchida, A. Kosugi, K. Miyake, T. Hamaoka, Effects of overexpression of PTP36, a putative protein tyrosine phosphatase, on cell adhesion, cell growth, and cytoskeletons in HeLa cells. *J. Biol. Chem.* **274**, 12905–12909 (1999).
23. C. Michaloglou, W. Lehmann, T. Martin, C. Delaunay, A. Hueber, L. Barys, H. Niu, E. Billy, M. Wartmann, M. Ito, C. J. Wilson, M. E. Digan, A. Bauer, H. Voshol, G. Christofori, W. R. Sellers, F. Hofmann, T. Schmelzle, The tyrosine phosphatase PTPN14 is a negative regulator of YAP activity. *PLOS One* **8**, e61916 (2013).
24. W. Wang, J. Huang, X. Wang, J. Yuan, X. Li, L. Feng, J. I. Park, J. Chen, PTPN14 is required for the density-dependent control of YAP1. *Genes Dev.* **26**, 1959–1971 (2012).
25. J. M. Huang, I. Nagatomo, E. Suzuki, T. Mizuno, T. Kumagai, A. Berezov, H. Zhang, B. Karlan, M. I. Greene, Q. Wang, YAP modifies cancer cell sensitivity to EGFR and survivin inhibitors and is negatively regulated by the non-receptor type protein tyrosine phosphatase 14. *Oncogene* **32**, 2220–2229 (2013).
26. P. A. Gregory, C. P. Bracken, E. Smith, A. G. Bert, J. A. Wright, S. Roslan, M. Morris, L. Wyatt, G. Farshid, Y. Y. Lim, G. J. Lindeman, M. F. Shannon, P. A. Drew, Y. Khew-Goodall, G. J. Goodall, An autocrine TGF-β/ZEB/miR-200 signaling network regulates establishment and maintenance of epithelial-mesenchymal transition. *Mol. Biol. Cell* **22**, 1686–1698 (2011).
27. R. M. Neve, K. Chin, J. Fridlyand, J. Yeh, F. L. Baehner, T. Fevr, L. Clark, N. Bayani, J. P. Coppe, F. Tong, T. Speed, P. T. Spellman, S. DeVries, A. Lapuk, N. J. Wang, W. L. Kuo, J. L. Stilwell, D. Pinkel, D. G. Albertson, F. M. Waldman, F. McCormick, R. B. Dickson, M. D. Johnson, M. Lippman, S. Ethier, A. Gazdar, J. W. Gray, A collection of breast cancer cell lines for the study of functionally distinct cancer subtypes. *Cancer Cell* **10**, 515–527 (2006).
28. A. J. Minn, G. P. Gupta, P. M. Siegel, P. D. Bos, W. Shu, D. D. Giri, A. Viale, A. B. Olshen, W. L. Gerald, J. Massagué, Genes that mediate breast cancer metastasis to lung. *Nature* **436**, 518–524 (2005).
29. P. Timpson, E. J. McGhee, Z. Erami, M. Nobis, J. A. Quinn, M. Edward, K. I. Anderson, Organotypic collagen I assay: A malleable platform to assess cell behaviour in a 3-dimensional context. *J. Vis. Exp.*, e3089 (2011).
30. J. A. Joyce, J. W. Pollard, Microenvironmental regulation of metastasis. *Nat. Rev. Cancer* **9**, 239–252 (2009).
31. B. Psaila, D. Lyden, The metastatic niche: Adapting the foreign soil. *Nat. Rev. Cancer* **9**, 285–293 (2009).
32. T. Tiganis, A. M. Bennett, Protein tyrosine phosphatase function: The substrate perspective. *Biochem. J.* **402**, 1–15 (2007).
33. G. G. Tall, M. A. Barbieri, P. D. Stahl, B. F. Horazdovsky, Ras-activated endocytosis is mediated by the Rab5 guanine nucleotide exchange activity of RIN1. *Dev. Cell* **1**, 73–82 (2001).
34. M. A. Barbieri, C. Kong, P. I. Chen, B. F. Horazdovsky, P. D. Stahl, The SRC homology 2 domain of Rin1 mediates its binding to the epidermal growth factor receptor and regulates receptor endocytosis. *J. Biol. Chem.* **278**, 32027–32036 (2003).
35. K. Deininger, M. Eder, E. R. Kramer, W. Zieglgänsberger, H. U. Dodt, K. Dornmair, J. Colicelli, R. Klein, The Rab5 guanylate exchange factor Rin1 regulates endocytosis of the EphA4 receptor in mature excitatory neurons. *Proc. Natl. Acad. Sci. U.S.A.* **105**, 12539–12544 (2008).
36. K. Balaji, C. Mooser, C. M. Janson, J. M. Bliss, H. Hojjat, J. Colicelli, RIN1 orchestrates the activation of Rab5 GTPases and ABL tyrosine kinases to determine the fate of EGFR. *J. Cell Sci.* **125**, 5887–5896 (2012).
37. A. Basu, D. Pal, Two faces of protein kinase Cδ: The contrasting roles of PKCδ in cell survival and cell death. *ScientificWorldJournal* **10**, 2272–2284 (2010).
38. S. R. Sampson, D. R. Cooper, Specific protein kinase C isoforms as transducers and modulators of insulin signaling. *Mol. Genet. Metab.* **89**, 32–47 (2006).
39. A. Lladó, P. Timpson, S. Vilà de Muga, J. Moretó, A. Pol, T. Grewal, R. J. Daly, C. Enrich, F. Tebar, Protein kinase Cδ and calmodulin regulate epidermal growth factor receptor recycling from early endosomes through Arp2/3 complex and cortactin. *Mol. Biol. Cell* **19**, 17–29 (2008).
40. M. Park, W. K. Kim, M. Song, M. Park, H. Kim, H. J. Nam, S. H. Baek, H. Kim, Protein kinase C-δ–mediated recycling of active KIT in colon cancer. *Clin. Cancer Res.* **19**, 4961–4971 (2013).
41. B. L. Allen-Petersen, C. J. Carter, A. M. Ohm, M. E. Reyland, Protein kinase Cδ is required for ErbB2-driven mammary gland tumorigenesis and negatively correlates with prognosis in human breast cancer. *Oncogene* **33**, 1306–1315 (2014).
42. P. Fang, Z. Zhao, H. Tian, X. Zhang, RIN1 exhibits oncogenic property to suppress apoptosis and its aberrant accumulation associates with poor prognosis in melanoma. *Tumour Biol.* **33**, 1511–1518 (2012).
43. H. F. Yu, G. Zhao, Z. J. Ge, D. R. Wang, J. Chen, Y. Zhang, T. Z. Zha, K. Zhang, M. Zhang, Y. F. Tan, S. J. Zhou, C. Jiang, High RIN1 expression is associated with poor prognosis in patients with gastric adenocarcinoma. *Tumour Biol.* **33**, 1557–1563 (2012).
44. G. Y. Shan, Z. Zhang, Q. G. Chen, X. Y. Yu, G. B. Liu, C. Z. Kong, Overexpression of RIN1 associates with tumor grade and progression in patients of bladder urothelial carcinoma. *Tumour Biol.* **33**, 847–855 (2012).
45. Q. Wang, Y. Gao, Y. Tang, L. Ma, M. Zhao, X. Wang, Prognostic significance of RIN1 gene expression in human non-small cell lung cancer. *Acta Histochem.* **114**, 463–468 (2012).
46. H. Hu, J. M. Bliss, Y. Wang, J. Colicelli, RIN1 is an ABL tyrosine kinase activator and a regulator of epithelial-cell adhesion and migration. *Curr. Biol.* **15**, 815–823 (2005).
47. X. Cao, K. Q. Tanis, A. J. Koleske, J. Colicelli, Enhancement of ABL kinase catalytic efficiency by a direct binding regulator is independent of other regulatory mechanisms. *J. Biol. Chem.* **283**, 31401–31407 (2008).
48. X. Li, S. Roslan, C. N. Johnstone, J. A. Wright, C. P. Bracken, M. Anderson, A. G. Bert, L. A. Selth, R. L. Anderson, G. J. Goodall, P. A. Gregory, Y. Khew-Goodall, MiR-200 can repress breast cancer metastasis through ZEB1-independent but moesin-dependent pathways. *Oncogene* **33**, 4077–4088 (2014).
49. F. Hochgräfe, L. Zhang, S. A. O'Toole, B. C. Browne, M. Pinese, A. Porta Cubas, G. M. Lehrbach, D. R. Croucher, D. Rickwood, A. Boulghourjian, R. Shearer, R. Nair, A. Swarbrick, D. Faratian, P. Mullen, D. J. Harrison, A. V. Biankin, R. L. Sutherland, M. J. Raftery, R. J. Daly, Tyrosine phosphorylation profiling reveals the signaling network characteristics of basal breast cancer cells. *Cancer Res.* **70**, 9391–9401 (2010).
50. J. Cox, N. Neuhauser, A. Michalski, R. A. Scheltema, J. V. Olsen, M. Mann, Andromeda: A peptide search engine integrated into the MaxQuant environment. *J. Proteome Res.* **10**, 1794–1805 (2011).
51. J. Schindelin, I. Arganda-Carreras, E. Frise, V. Kaynig, M. Longair, T. Pietzsch, S. Preibisch, C. Rueden, S. Saalfeld, B. Schmid, J. Y. Tinevez, D. J. White, V. Hartenstein, K. Eliceiri, P. Tomancak, A. Cardona, Fiji: An open-source platform for biological-image analysis. *Nat. Methods* **9**, 676–682 (2012).
52. R. Roskoski, ERK1/2 MAP kinases: Structure, function, and regulation. *Pharmacol. Res.* **66**, 105–143 (2012).
53. E. Kida, M. Walus, K. Jarząbek, S. Palminiello, G. Albertini, A. Rabe, Y. W. Hwang, A. Golabek, A form of dual-specificity tyrosine-(Y)-phosphorylation-regulated kinase 1A nonphosphorylated at tyrosine 145 and 147 is enriched in the nuclei of astroglial cells, adult hippocampal progenitors, and some cholinergic axon terminals. *Neuroscience* **195**, 112–127 (2011).
54. K. Balaji, C. Mooser, C. M. Janson, J. M. Bliss, H. Hojjat, J. Colicelli, RIN1 orchestrates the activation of Rab5 GTPases and ABL tyrosine kinases to determine EGFR fate. *J. Cell Sci.* **125**, 5887–5896 (2012).
55. H. Shen, S. M. Ferguson, N. Dephoure, R. Park, Y. Yang, L. Volpicelli-Daley, S. Gygi, J. Schlessinger, P. De Camilli, Constitutive activated Cdc42-associated kinase (Ack) phosphorylation at arrested endocytic clathrin-coated pits of cells that lack dynamin. *Mol. Biol. Cell* **22**, 493–502 (2011).
56. C. Corti, E. Leclerc L'Hostis, M. Quadroni, H. Schmid, I. Durussel, J. Cox, P. Dainese Hatt, P. James, E. Carafoli, Tyrosine phosphorylation modulates the interaction of calmodulin with its target proteins. *Eur. J. Biochem.* **262**, 790–802 (1999).
57. S. Himpel, P. Panzer, K. Eirmbter, H. Czajkowska, M. C. P. L. Sayed, T. Blundell, H. Kentrup, J. Gro, Identification of the autophosphorylation sites and characterization of their effects in the protein kinase DYRK1A. *J. Biochem.* **505**, 497–505 (2001).
58. K. Hughes, E. Nikolakaki, S. E. Plyte, N. F. Totty, J. R. Woodgett, Modulation of the glycogen synthase kinase-3 family by tyrosine phosphorylation. *EMBO J.* **12**, 803–808 (1993).
59. N. K. Prasad, M. E. Werner, S. J. Decker, Specific tyrosine phosphorylations mediate signal-dependent stimulation of SHIP2 inositol phosphatase activity, while the SH2 domain confers an inhibitory effect to maintain the basal activity. *Biochemistry* **48**, 6285–6287 (2009).
60. J. De Schutter, A. Guillabert, V. Imbault, C. Degraef, C. Erneux, D. Communi, I. Pirson, SHIP2 (SH2 domain-containing inositol phosphatase 2) SH2 domain negatively controls SHIP2 monoubiquitination in response to epidermal growth factor. *J. Biol. Chem.* **284**, 36062–36076 (2009).
61. L. Delahaye, I. Mothe-Satney, M. G. Myers, M. F. White, E. Van Obberghen, Interaction of insulin receptor substrate-1 (IRS-1) with phosphatidylinositol 3-kinase: Effect of substitution of serine for alanine in potential IRS-1 serine phosphorylation sites. *Endocrinology* **139**, 4911–4919 (1998).

62. J. Bao, I. Alroy, H. Waterman, E. D. Schejter, C. Brodie, J. Gruenberg, Y. Yarden, Threonine phosphorylation diverts internalized epidermal growth factor receptors from a degradative pathway to the recycling endosome. *J. Biol. Chem.* **275**, 26178–26186 (2000).

Acknowledgments: We thank J. Massague for the MDA-MB-231 LM2 cell line, S. Pitson for the EF1A1 cDNA, C. Mitchell for the INPPL1 cDNA, J.-W. Soh for PRKCD-GFP cDNA, C. Larsson for PRKCD cDNA, and G. Secker and N. Harvey for assistance with lymphatic endothelial cells. **Funding:** This work was supported by project grants from the National Health and Medical Research Council (NHMRC), Australia (626918), Cancer Council of South Australia (508105, 399320), and the Kid's Cancer Project to Y.K.-G. Y.K.-G. was a recipient of a Cancer Council of South Australia Senior Research Fellowship. L. Belle (nee Wyatt) was a recipient of an Australian Postgraduate Award and a Royal Adelaide Hospital Dawes Postgraduate Top-up Scholarship. R.J.D. was supported by a Fellowship (535914) and Program Grant (535903) from the NHMRC. **Author contributions:** L.B., A.L., P.T., R.J.D., and Y.K.-G. conceived the project; L.B., N.A., A.L., X.L., J.L.P., S.R., D.H., J.R.W.C., F.K.G., A.G.B., and L.A.C. conducted experiments; A.T. provided the analysis used to generate Fig. 6; L.B., N.A., A.L., G.F., G.J.G., P.T., R.J.D., and Y.K.-G. analyzed the data; and L.B., N.A., A.L., R.J.D., and Y.K.-G. wrote the paper. **Competing interests:** The authors declare that they have no competing interests. **Data and materials availability:** The raw mass spectrometry data have been deposited to Proteome Xchange Consortium, www.ebi.ac.uk/pride, data set identifier PXD001739.

Submitted 30 May 2014
Accepted 28 January 2015
Final Publication 17 February 2015
10.1126/scisignal.2005547
Citation: L. Belle, N. Ali, A. Lonic, X. Li, J. L. Paltridge, S. Roslan, D. Herrmann, J. R. W. Conway, F. K. Gehling, A. G. Bert, L. A. Crocker, A. Tsykin, G. Farshid, G. J. Goodall, P. Timpson, R. J. Daly, Y. Khew-Goodall, The tyrosine phosphatase PTPN14 (Pez) inhibits metastasis by altering protein trafficking. *Sci. Signal.* **8**, ra18 (2015).

The tyrosine phosphatase PTPN14 (Pez) inhibits metastasis by altering protein trafficking

Leila Belle, Naveid Ali, Ana Lonic, Xiaochun Li, James L. Paltridge, Suraya Roslan, David Herrmann, James R. W. Conway, Freya K. Gehling, Andrew G. Bert, Lesley A. Crocker, Anna Tsykin, Gelareh Farshid, Gregory J. Goodall, Paul Timpson, Roger J. Daly and Yeesim Khew-Goodall (February 17, 2015)
Science Signaling **8** (364), ra18. [doi: 10.1126/scisignal.2005547]

Science Signaling (ISSN 1937-9145) is published weekly, except the last December, by the American Association for the Advancement of Science, 1200 New York Avenue, NW, Washington, DC 20005.